### Title

Nonmetal to Metal Transition and Ultrafast Charge Carrier Dynamics of Zn Clusters on p-Si(100) by fs-XUV Photoemission Spectroscopy




### Journal

Nano Letters, 18(7)

### ISSN

1530-6984



### Authors

Vaida, Mihai E
Marsh, Brett M
Leone, Stephen R



### Publication Date

2018-07-11

### DOI

10.1021/acs.nanolett.8b00700

# Non-metal to metal transition and ultrafast charge carrier dynamics of Zn clusters on p-Si(100) by fs-XUV photoemission spectroscopy

Mihai E. Vaida[1,2,*], Brett M. Marsh[1], and Stephen R. Leone[1,3,4,*]

[1] Department of Chemistry, University of California, Berkeley, California 94720, United States
[2] Department of Physics and Energy Conversion and Propulsion Cluster, University of Central Florida, Florida 32816, United States
[3] Department of Physics, University of California, Berkeley, California 94720, United States
[4] Chemical Sciences Division, Lawrence Berkeley National Laboratory, Berkeley, California 94720, United States

## Abstract

Understanding the electronic structure and charge carrier dynamics of supported clusters is important due to their many potential applications in photochemistry and catalysis. In this investigation, photoemission spectroscopy, in conjunction with femtosecond extreme ultraviolet (XUV) laser pulses, is used to investigate the electronic structure and ultrafast charge carrier dynamics at a Si(100) surface decorated with Zn clusters. Static photoemission spectroscopy is used to investigate the changes in the electronic structure as the dimensionality of the Zn is increased from small clusters composed of a very few atoms to metallic Zn particles. Furthermore, femtosecond optical-pump XUV-probe photoemission spectroscopy is employed to induce a charge transfer from the p-Si(100) substrate to the Zn clusters and to measure in real time the charge trapping at the Zn cluster as well as the subsequent charge relaxation. The ultrafast charge carrier dynamics are also investigated for small clusters and metallic Zn particles. Significant transient charging of the Zn clusters after excitation of the Si(100) substrate by 800 nm light is observed for Zn coverages greater than 0.12 ML Zn, which coincides with the formation of a Schottky barrier at the interface between the Zn particle and the p-Si(100)

---

*) Authors to whom correspondence should be addressed. E-mail: mihai.vaida@ucf.edu, Tel: +1 407-823-4213 and E-mail: srl@berkeley.edu, Tel: +1 510-643-5467

substrate. The transient signals show that the charge trapping time at the Zn cluster varies with the cluster size, which is rationalized based on the electronic structure of the cluster as well as the band energy alignment at the Zn cluster-Si(100) junction.

***Keywords: Ultrafast Spectroscopy, Schottky Junction, Metal Clusters, XUV Spectroscopy, Photoemission***

Nanostructured materials consisting of semiconductor substrates decorated with small clusters or nanoparticles have many potential applications in photocatalysis, such as the generation of storable fuels from sustainable inputs,[1-4] antibacterial action,[5-7] and degradation of organic pollutants. The fate of a photocatalytic reaction is drastically influenced by the electronic structure of the metal clusters as well as the energy band alignment at the interface between the cluster and surface. The overall process on a photocatalytic material composed of a semiconductor decorated with metal particles occurs in three steps.[2] First, by means of light irradiation at an energy equal to or greater than the band gap of the semiconductor, electrons are excited from the valence band into the conduction band, leaving holes in the valence band. Second, these charges separate and migrate to the surface, where the electrons attach to the metal clusters. Third, the excess electrons in the metal clusters and the holes at the semiconductor surface promote reduction and oxidation reactions, respectively.[2] A fast charge separation and transport to the surface and subsequently a long recombination time of the charged particles are beneficial for an efficient photocatalytic material. Therefore, understanding the electronic structure and ultrafast photoinduced charge carrier dynamics at the cluster-surface interface is a defining principle that will guide advances in the field of photocatalysis.

The electronic structure of various metal cluster sizes and compositions, in gas phase or attached to solid surfaces, has been extensively investigated using various techniques, such as photoelectron spectroscopy[10-12] and scanning tunneling spectroscopy.[13-15] Moreover, the dynamics that occur in metal nanoparticles in solutions or embedded in matrices have also been investigated for various particle sizes and compositions using pump-probe transient absorption spectroscopy in conjunction with femtosecond laser pulses.[16] A significant emphasis is placed on understanding the sequences of events following light absorption and

their time scales, i.e. electron-electron scattering (within a few hundred femtoseconds),[17-21] electron-phonon interaction (a few picoseconds), and energy dissipation to the surroundings (hundreds of picoseconds).

In contrast to the vast number of time-resolved investigations on metal particles in solutions or embedded in matrices, there is a lack of information regarding the ultrafast charge carrier dynamics at metal clusters on solid surfaces. This might be due to the limited investigative techniques that can offer time resolution, surface sensitivity, and element specificity. All these requirements are fulfilled by an experimental technique used in the present investigation that combines pump-probe photoelectron spectroscopy with femtosecond extreme ultraviolet (XUV) laser pulses.

This paper discusses breakthroughs in measuring electronic structure and ultrafast charge carrier dynamics at the surface of a model photocatalytic system consisting a p-type doped Si(100) surface decorated with Zn clusters. Static XUV photoemission spectroscopy is utilized to monitor the electronic structure of Zn clusters on p-Si(100) as a function of Zn deposition under ultrahigh vacuum conditions. Furthermore, the femtosecond pump-probe XUV photoemission spectroscopy technique is employed to induce a charge transfer from the p-Si(100) substrate to the Zn clusters and to measure in real time the charge trapping at the Zn cluster as well as the subsequent charge relaxation. Ultrafast charge carrier dynamics is investigated as the Zn dimensionality is increased from small clusters composed of a very few atoms to larger particles that have a metallic character.

The experimental apparatus employed in the present investigations consists of (i) a commercial amplified fs laser system in conjunction with a pump-probe setup, (ii) a table top pulsed XUV source based on high harmonic generation (HHG) coupled to a home-built XUV monochromator, and (iii) an ultra high vacuum (UHV) surface science chamber. Fig. 1 shows a schematic representation of the XUV source, XUV wavelength-selection

monochromator, and the UHV surface science chamber. Briefly, the fs-laser pulses are produced by a Ti:sapphire laser system (KM Labs) to yield 24 fs pulses at a central wavelength of 800 nm, a typical average power of 2.2 W, and a repetition rate of 1 kHz. The amplified laser beam is divided into two arms to produce the pump and the probe laser beams. In the present investigation the fundamental wavelength, i.e. 800 nm, is used as a pump pulse to excite silicon through the indirect band gap. The XUV probe laser beam is produced by focusing the 800 nm infrared (IR) beam to $10^{14}$-$10^{15}$ W $cm^{-2}$ in a semi-infinite gas cell filled with Ar (cf. HHG cell in Fig. 1). The generated harmonics co-propagate with the residual fundamental laser light. The harmonics are spectrally dispersed by a plane grating and one harmonic is selected and subsequently focused on the sample in the middle of surface science chamber by a cylindrical mirror and a toroidal mirror at grazing incidence. An aluminum mirror installed inside of the vacuum apparatus a few millimeters above the XUV beam (cf. inset in Fig. 1) is used to steer the pump laser beam into the UHV chamber and to ensure the overlap between the pump and the probe beams onto the sample surface. The angle between the pump and the probe beam is about 1.5°. The sizes of the IR-pump and XUV-probe laser beams on the sample are about 1 mm and 0.2 mm, respectively. The apparatus time response function obtained via laser assisted photoemission (LAPE)[26-28] is 80 fs ±15.

The UHV surface science chamber contains specific tools for surface preparation and characterization such as an $Ar^+$ gun for surface cleaning, a thermal evaporator used for the preparation of Zn particles, an Auger electron spectrometer (AES) to investigate the surface composition and cleanliness, and a time-of-flight (TOF) photoelectron spectrometer (PES) to investigate the electronic structure and the electron dynamics at surfaces. For the photoemission experiments, the surface sample is positioned perpendicular to the TOF spectrometer axis at a distance of 8 mm from the first TOF spectrometer electrode. A negative bias potential of -10 V is applied

on the sample to repel and guide the photoelectrons toward the spectrometer.

The sample surface is attached to a liquid nitrogen cryostat, which is mounted in the center of the UHV chamber and achieves a low temperature of 90 K. An X,Y,Z,θ mechanical manipulator is employed for positioning the sample in front of the preparation and characterization tools. The base pressure of the UHV surface science chamber is $1.5\times10^{-10}$ Torr. During the XUV photoemission experiments the pressure in the UHV chamber rises to $2.0\times10^{-10}$ Torr due to the residual Ar gas originating from the HHG source.

In this investigation a p-doped Si(100) substrate with a resistivity of 100 Ω-cm is employed. Initially, the substrate is cleaned by several cycles of $Ar^+$ sputtering (0.5 keV, 7 μA) for 20 min followed by 5 min of annealing at 600 K. The sputtering-annealing cycles are performed until no oxygen, carbon or other contaminants are detected via AES. Zn clusters or Zn thin films are prepared using a home-built Zn metal evaporator consisting of a Zn ribbon with purity of 99.99% wrapped in a tantalum heating wire. The Zn evaporation rate of 0.20 ML/min was determined via AES as described in our previous investigations. The Zn clusters and thin films are synthesized by evaporating well-defined amounts of Zn at normal incidence on the p-Si(100) surface. The p-Si(100) substrate is maintained at 90 K at all times during the preparation and characterization of the samples to minimize surface diffusion and modification by the laser pulses.[30]

As demonstrated in our previous investigations, fs-XUV photoemission spectroscopy is not just a surface sensitive technique, but it also one of the most sensitive methods that can be used to monitor with high precision the electronic structure and oxidation state as well as the density of defects at surfaces. In the present investigation, static fs-XUV photoemission spectroscopy is used to monitor the electronic structure of Zn clusters on the Si substrate.

Figure 2 displays photoemission spectra obtained using the 27$^{th}$ harmonic (41.85 eV) from various amounts of Zn evaporated on the p-Si(100) surface. The 27$^{th}$ harmonic bandwidth of 1.8 eV at FWHM limits the energy resolution of the photoemission spectra. The binding energy in Figure 2 is referenced to the Fermi level ($E_F$ = 0), which is at the center of the Fermi Dirac distribution that fits the photoemission of the Ta metal clips, which holds the sample. Specifically, the model of Lu and coworkers[31] is used, which convolutes the Fermi-Dirac distribution with a Gaussian that accounts for broadening due to instrumental resolution and the width of the photoemission source. The photoemission spectrum obtained from the p-Si(100) substrate in the binding energy region of 0 to -12 eV is shown in Figure 2(a). The valence band maximum (VBM) of the p-Si(100) substrate, which is at 0.37 eV below the $E_F$ (larger negative numbers refer to greater binding energies). In the binding energy region investigated here, the photoemission spectrum of Si is featureless.

When 0.02 ML Zn is evaporated on the p-Si(100) substrate, the photoemission spectrum at low binding energies remains the same as the one obtained from the bare Si substrate, (cf. inset in Figure 2(a), but a new peak is detected at a binding energy of -9.80 eV. No change in the photoemission onset is observed for a Zn coverage of 0.04 ML, but the peak at higher binding energy increases in intensity and shifts to -9.73 eV. When the Zn coverage is increased to 0.07 ML the photoemission onset shifts by -0.17 eV, and the -9.80 eV peak shifts slightly more toward lower binding energies. A similar result is obtained for a coverage of 0.12 ML Zn. For a coverage of 0.16 ML Zn, as well as for all the higher coverages investigated, the photoemission onset shifts to an even lower binding energy, which coincided with the onset of the photoemission recorded from the Ta clips. The photoemission peak around -9.8 eV continuously shift to lower binding energy as the Zn coverage increases. The magnitude of the peak shift decreases asymptotically as the Zn thickness is approaching the mean free path of the photoelectrons .

The peak observed around -9.8 eV is due to the photoemission from the 3d electronic states of the Zn evaporated on the p-Si(100) substrate.[32] Its intensity is directly related to the amount of Zn on the p-Si(100) substrate. The shift of the Zn 3d peak as a function of the Zn loading can be attributed to a change in the electronic environment of Zn due to the formation of larger and larger Zn particles. For additional clarity, Figures S1 and S2 in the Supporting Information display the shifts of the Zn-3d peak and photoemission onset as a function of Zn coverage. At small Zn coverages up to 0.16 ML, the area of the Zn-3d peak increases linearly with the amount of Zn evaporated on Si(100) as indicated by the red line in Figure S3. For higher coverages, i.e. 0.45 ML to 3 ML, the area of the Zn-3d peak still increases with the Zn loading, but at a slower rate. The non-linear increase of the Zn-3d area with the coverage is attributed to the formation of 2 ML patches of Zn on the Si(100). We expect that the Zn-3d peak area will not further increase with the Zn coverages after the Zn film is thicker than the penetration depth of the photoelectrons produced with the XUV laser pulses.

While no STM investigations are performed here, in previous scanning tunneling microscopy (STM) investigations, Tanaka et al. observed that Zn monomers, dimers and trimers are formed when 0.04 ML of Zn are evaporated on Si(111).[33] In a similar investigation, Xie and Tanaka observed Zn nano-rows oriented in the [110] direction of a Si(100)-2 × 1 substrate when 0.2 ML of Zn are evaporated on the surface at room temperature.[34] Furthermore, increasing the amount of Zn to 0.5 ML and 1 ML results in the formation of large flat Zn particles and 3D particles, respectively. Various other STM investigations demonstrate that evaporation of metals in the range of 0.02-0.04 ML on substrates held at ≤100 K result in surfaces decorated with mostly atoms, because at these low temperatures the metal atoms are immobile even on defect free unreactive substrates. In a recent investigation performed in our laboratory, we observed that Zn films deposited on p-type Si(100) at nominally liquid nitrogen temperature (90 K) grows in a layer-by-layer fashion.[30]

Based on the STM investigation of Tanaka et al.,[33] we expect that in the present experiment, the evaporation of 0.02 ML of Zn would lead to a surface decorated with mostly Zn monomers. Therefore, the large binding energy of the Zn 3d electrons obtained from 0.02 ML Zn on Si(100) (cf. Figure 2) reflect the Zn atoms bound to the Si atoms of the substrate. The shift of the Zn 3d peak to lower binding energies when the amount of Zn is increased to 0.04 ML (cf. Figure 2) indicates a change in the electronic structure of Zn, most probably due to the formation of small Zn clusters such as dimers and trimers, as observed by Tanaka et al.[33] at a similar Zn coverage. Accordingly, the shift of the Zn 3d peak to lower binding energies by increasing the Zn coverage indicates that some of the Zn atoms are not only bound to the Si(100) substrate, but also to some neighboring Zn atoms. Consequently, the shift of the Zn 3d peak in Figure 2 is a direct indication that larger and larger Zn cluster and particles are formed as the Zn coverage is increased. No shift of the Zn 3d peak is observed in the Figure 2 for coverages higher than 0.45 ML Zn. This is attributed to the formation of large particles, for which numerous Zn atoms are bound to other Zn atoms as in the bulk material.

The photoemission onsets in Figure 2(a) provide further details about the electronic structure of the Zn clusters at the Si(100) surface. In general, the highest occupied electronic states in non-metallic materials are below the Fermi level, while the first occupied electronic states in metals are at the Fermi level. Accordingly, the onsets of the photoemission spectra recorded from the lowest Zn coverages of 0.02 ML and 0.04 ML coincide with that of the bare Si(100) substrate and therefore the Zn clusters formed at these coverages have a non-metallic character. For 0.07 ML and 0.12 ML Zn coverages, the photoemission onsets are in the band gap of Si(100), indicating that the Zn particles at this coverage also do not have a metallic character. For all the Zn coverages of 0.16 ML or larger, however, the photoemission onsets shift above the Fermi level, similar with the photoemission from metals (cf. Figure S2 in Supporting Information). This

clearly indicates that particles formed by Zn coverages of 0.16 ML or greater have a metallic character. Consequently, the transition of Zn clusters from non-metal to metal on Si(100) occurs at Zn coverages between 0.13 - 0.16 ML.

To gain more insights into the electronic structure of the small Zn clusters and particles at the surface, we plotted in Figure 2(b) the difference between the photoemission spectra of Zn/Si(100) and the photoemission spectrum of the bare Si(100) substrate. The photoemission of 0.02 ML Zn shows a distinct peak at -0.90 eV as well as a double peak structure at -2 eV binding energy (cf. red filled spectrum in Figure 2(b)). For a coverage of 0.04 ML Zn, multiple distinct peaks are noticeable at binding energies between -0.3 and -2.0 eV, (cf. green filled spectrum in Figure 2(b)) in the difference photoemission spectrum. For higher Zn coverages, the peaks merge into broad photoemission features, which extend above the Fermi level. Also, a few distinct peaks are still visible at binding energies greater than -1.5 eV for the high Zn coverages.

The distinct photoemission peaks observed for 0.02 ML and 0.04 ML coverages of Zn (cf. Figure 2(b)) are attributed to the highest occupied molecular orbitals (HOMO) of small Zn clusters. Such discreet distributions of electronic states are characteristic for small Zn clusters composed of very few atoms, which have electronic structures similar to that of atoms and molecules.[39] The broad photoemission features observed when the Zn coverage is increased to 0.07 ML and 0.12 ML is attributed to the formation of electronic band structures due to the large number of atoms in each Zn cluster. For Zn coverages of 0.16 ML or higher, these broad photoemission features extend above the Fermi level, due to the formation of Zn particles with a metallic character, as mentioned above.

The shifts of the Zn-3d peak and photoemission onset as the Zn coverage is increased (cf. Figure 2), can be also influenced by a change in the electronic structure of the p-Si(100) substrate, due to the reduction of the band bending at the surface. Such a band flattening due to the presence

of the Zn particles would equally influence every feature present in the photoemission spectra. Therefore, to see the influence of the p-Si(100) band flattening due to the presence of the Zn particles, the shift of the secondary electron cut-off has been compared with the shifts of Zn-3d peak and the photoemission onset as the Zn coverage is increased (see Figure S2 in the Supporting Information). The maximum shift of the secondary electron cut-off toward lower binding energies as the Zn coverage is increased has a value of 0.06 eV, which indicates that the p-Si(100) band flattening plays just a minor role in the shifts of the Zn-3d peak and photoemission onset.

The ultrafast charge carrier dynamics at the Zn particles attached to the Si(100) substrate is further investigated employing a pump-probe schema, which is illustrated in Figure 3(a). An IR-pump laser pulse at the central wavelength of 800 nm (1.55 eV) is used to excite electrons from the valence band into the conduction band in the indirect band gap transition of p-Si(100), leaving holes in the valence band. We chose a p-type doped Si(100) substrate for this investigation, because in the space charge region, close to the semiconductor surface, its bands are bent downward, i.e. away from the vacuum level, which consequently facilitates the migration of the photoexcited electrons to the surface. Therefore, immediately after the pump laser pulse photoexcitation, the electrons in the conduction band of p-Si(100) are accelerated toward the surface while the holes in the valence band are accelerated toward the bulk of the p-Si(100) substrate. The electrons at the p-Si(100) surface can attach to the Zn particles, resulting in a transient negative charging of these particles, which further leads to a transient shift of the whole electronic structure of the particle towards lower binding energies (smaller negative numbers versus the Fermi energy). Subsequently, the XUV-probe laser pulse, i.e. 23$^{rd}$ harmonic (35.65 eV, FWHM of 1.45 eV) detects the presence of excess electrons at the Zn particles by monitoring the transient shift of the unambiguous Zn 3d photoemission peak as a function of the pump-probe time delay.

Figure 3(b) displays photoemission spectra recorded for 0.12 ML Zn/Si(100) at -3 ps and 1.2 ps pump-probe time delay, in the binding energy region of the Zn 3d peak. At negative time delay the XUV-probe laser pulse arrives at the sample surface before the IR-pump laser pulse, while at positive time delay the sequence of the laser pulses is exchanged, i.e., IR-pump is followed by the XUV-probe. The shift of the Zn 3d peak at 1.2 ps in Figure 3(b) clearly shows that the Zn particles become negatively charged after the pump pulse photoexcitation. In this scenario, the observed shift is directly a result of the transfer of electrons from the p-Si substrate to the Zn overlayer. As electrons populate the surface, the electron Fermi level increases in energy in the Zn layer, as expected from Fermi-Dirac statistics. This shift moves the electrons in Zn closer to the vacuum level, meaning that the amount of energy needed to liberate photoelectrons is lowered. The shift of the Fermi level similarly influences the energetic position of the Zn 3d core level, leading to a decrease in the observed Zn 3d electron binding energy after photoexcitation. Such changes in the position of the Fermi level can only arise from changes in the electron population, while changes in the electron energy distribution simply result in the broadening of the distribution, not a change in the central energy

For the pump-probe measurements, the IR-pump laser fluence is maintained at $5x10^9$ W/cm$^2$ (10 mW average power, 25 fs, spot size of 1 mm). At this pump laser peak power density, a very small photoemission signal of a few counts per 1000 laser pulses is produced by the IR pump laser beam alone in the case of both bare and Zn decorated Si(100). This, however, indicates that the pump laser pulse can produce some multiphoton excitation, and, most likely, the excitation of the both direct and indirect band gaps of silicon. Direct multiphoton excitation of the Zn clusters by the IR-pump laser pulse is also possible. However, both these excitation processes would not be expected to lead to an excess of electrons in the Zn clusters and consequently to a transient shift of the Zn 3d peak to lower binding energies, as observed in the experiment. Therefore, these excitation

mechanisms are excluded. Furthermore, the pump-laser power employed in this experiment did not induce any change in the electronic structure of the surfaces investigated in this work. This indicates that heating effects that could modify the samples due to the long time exposure to the IR beam are negligible.

Experiments performed at high pump laser powers could lead to pump-induced space charge effects that might alter the observed transient signals due to the repulsion between the photoelectrons produced by the pump-alone, probe-alone, and pump plus probe laser pulses.[42] This space charge repulsion effect at high pump powers can also induce a broadening of the photoelectron spectra. However, such space charging effects are not observed at the pump laser power used in this experiment.

Figure 4 displays transient signals from 0.03 ML, 0.12 ML, and 0.2 ML Zn on Si(100), obtained by monitoring the Zn 3d photoemission peak shift as a function of the pump-probe time delay. These samples correspond to the most relevant three cases, i.e. small Zn clusters composed of a few atoms (0.03 ML), large nonmetallic Zn particles (0.12 ML) as well as large Zn particles that have a metallic character (0.2 ML). For each data point displayed in Figure 4, a photoemission spectrum is summed using 500000 laser pulses. The stability of the laser system and data acquisition reproducibility is checked during the transient by recording a reference spectrum at -3 ps pump-probe time delay after every two photoemission spectra. The errors obtained in the binding energy shifts are below ±15 meV. Figure 4 also displays a transient recorded from the bare p-Si(100) substrate, in which the shift of the valence band maximum of Si, i.e. the photoemission onset, is monitored as a function of the pump-probe time delay employing the same measurement conditions as for the samples consisting of Zn/p-Si(100). No transient shift of the p-Si(100) valence band maximum is observed, indicating that the surface photovoltage is negligible for the doping level of the substrate and the pump intensity used in this experiment.

No shift of the Zn 3d peak is observed for the 0.03 ML Zn/p-Si(100) (cf. filled circles in Figure 4). For the 0.12 ML Zn /Si(100) sample, a shift of the Zn 3d peak by a maximum of 0.12 eV is observed. Monitoring the binding energy shift of the Zn 3d peak maximum as a function of the pump-probe time delay leads to a transient signal (cf. open squares in Figure 4) that rises exponentially, reaches a maximum at 1.2 ps, and subsequently decays. The best fit to the measured data by an exponential rise followed by a single exponential decay convoluted with the instrumental time response function leads to a time constant of $\tau_{1(rise)}$= 0.55 ± 0.1 ps for the rise and a $\tau_{2(decay)}$ = 2 ± 0.5 ps for the decay (cf. Figure 4). The rise time constant is attributed to the migration of photoexcited electrons from the conduction band of the p-Si(100) substrate to the unoccupied electronic states of the Zn particles. In a previous investigation performed in this laboratory, in which the electron transfer from a p-Si(100) substrate to an oxygen deficient (defect rich) n-$TiO_2$ ultrathin film was monitored in real time via XUV pump-probe photoemission spectroscopy, a similar rise time constant (450 ± 50 fs) and position of the transient peak maximum (1.2 ps) were measured.[30] In both investigations the same type of p-Si(100) substrate, i.e. same doping element and dopant concentration, were used and similar time constants for the charge transfer from the substrate to the adsorbate were obtained. Therefore, we consider that this initial time constant mostly reflects the migration of the electrons from the bulk to the surface of the p-Si(100) substrate, while the electron transfer time between p-Si(100) and the interface material is negligible.

The subsequent decay of the transient signal with a time constant of 2± 0.5 ps is attributed to the recombination of the excess electrons in the Zn particles with the holes present in the substrate. Intriguingly, by increasing the amount of Zn to 0.2 ML on the p-Si(100) surface, the recombination time constant increases to 26 ±3 ps. It needs to be mentioned that the best fit to the transient signal from 0.2 ML Zn on Si(100) is obtained by a single exponential decay convoluted with the instrumental time response function

as in the case of 0.12 ML Zn on Si(100). A very accurate fit cannot be obtained by a single exponential decay function nor by a biexponential decay function due to the large errors in the data points.

To explain the large increase in the time constant by increasing the amount of Zn on the substrate, as well as to explain why no charge transfer is observed when the p-Si(100) substrate is decorated with small Zn clusters, i.e. 0.03 ML Zn, the electronic structure of the Zn particle-p-Si(100) system is considered. Figure 5 displays three example energy band diagrams for the samples investigated in Figure 4, i.e. p-Si(100) substrate decorated with Zn small clusters (0.03 ML Zn), large non-metallic Zn particles (0.12 ML Zn), and metallic Zn particles (0.2 ML Zn). The energy band alignments are constructed using the valence band maximum (VBM) energy of p-Si(100) and the occupied electronic states of Zn measured in this work, as well as the literature values for the band gap energy of the Si,[43] the vacuum levels of Si[44] and polycrystalline Zn, and the ionization potential of small Zn clusters.[47]

In the case of small Zn clusters on p-Si(100), the band energy diagram in Figure 5(a) indicates that the occupied electronic states in the small Zn clusters are below the valence band maximum of p-Si(100) (cf. also Figure 2(b)). In this case, electrons from the valence band of the p-Si(100) substrate can migrate unrestricted to the Zn clusters. Therefore, a partial charging of the small Zn clusters is possible immediately after Zn adsorption on the p-Si(100) without any need for substrate photoexcitation. Such a charging of the small metal cluster immediately after adsorption on solid substrates is evident in various investigations and explains various heterogeneous catalytic reactions at surfaces decorated with small metal clusters. The absence of a transient signal from small Zn clusters can also be explained by their lowest unoccupied molecular orbitals, which can be resonant with the conduction band of the p-Si(100) substrate, but might not be populated due to their high energy, which cannot be reached by the pump photons. Furthermore, the lifetime of the lowest unoccupied molecular orbitals of the Zn clusters might be too short to be detected in our experimental setup.

For a Zn coverage of 0.12 ML, a Schottky barrier is formed at the interface between the Zn particle and the p-Si(100) substrate, because the first occupied electronic states in the 0.12 ML Zn particles are higher in energy than the valence band maximum of p-Si(100), as observed in the photoemission experiment (cf. Figure 2(b)) and schematically represented in Figure 5(b). This Schottky barrier hinders the electron migration from the valence band of the p-Si(100) substrate to the 0.12 ML Zn particles. The height of the barrier increases up to 0.37 eV as the amount of Zn is increased to 0.2 ML and metallic clusters are formed.[30] When large metallic Zn particles are formed on the p-Si(100) substrate, their unoccupied band electronic structure can be favorable to create a built-in electric field at the Zn-Si(100) interface, so that photoexcited electrons from the conduction band of Si(100) can move toward the Zn particle.[50]

The decay time constants obtained in this experiment, which increase with the Zn cluster size, follow the same trends observed in other time-resolved experiments employing transient absorption spectroscopy on metal nanoparticles in solutions or embedded in solid matrices (ref and refs therein). In those transient absorption experiments, in which various metal particles, i.e. Au, Ag, Ga, Sn, etc, are photoexcited, increases in the electron-electron, electron-phonon, and phonon-phonon coupling time constants with metal particle size are observed. However, in the current experiment, the light excites the p-Si(100) substrate and the electrons are transferred to the Zn clusters and subsequently recombine with the holes left in the substrate. Therefore, the time constant for transfer to the Zn clusters, i.e. the rise time constant obtained from Figure 4, as well as the recombination time constants, are longer than the time constants observed in those other transient absorption experiments. The shorter decay time constant obtained in this experiment for small clusters i.e. 0.12 ML Zn vs 0.20 ML Zn, can be attributed to a faster energy transfer back to the substrate, because smaller particles have larger surface to volume ratios, which leads to a faster relaxation.[52] Hartland and coworkers[53] observed that for small Au clusters,

the time scale for energy transfer from the cluster to the environment is competitive with the time scale for electron-phonon coupling, i.e. a few picoseconds, while for large Au particles hundreds of picoseconds are necessary to achieve total relaxation. Moreover, in the present experiment, the Zn clusters can also act as recombination centers for charged particles. If the electron-hole recombination occurs at the surface of the clusters, the small clusters will mediate the recombination more efficiently because of their larger surface to volume ratio. Furthermore, the relaxation time constant of the Zn particles might also be related to the lifetime of the unoccupied electronic states of the Zn particles in which the photoexcited electrons from silicon are transferred.

The increase in the magnitude of the transient signal intensity by a factor of about 10 as the Zn coverage is increased from 0.12 ML to 0.2 ML is attributed to an accumulation of a large number of electrons in the Zn metallic particles. Such large transient shifts have been recently observed in a Zn ultrathin layer on a p-Si(100) substrate and rationalized based on the energetics of band flattening and carrier accumulation in the metallic layer of the Zn/p-Si(100) heterojunction at high carrier densities.[30]

In this work, static fs-XUV photoemission spectroscopy has been employed to monitor the evolution of the electronic structures of Zn clusters as their dimensionality is increased from small clusters composed of a very few atoms to large particles and extended Zn films.[30] At very low Zn coverages, distinct photoemission peaks are observed, indicating that the Zn clusters have electronic structures similar to atoms and molecules. As the Zn coverage is increased, the XUV photoelectron spectra reveal an increase in the density of occupied electronic states in Zn, which subsequently leads to the formation of a band structure in clusters. The non-metal to metal transition is observed at a Zn coverage of 0.16 ML by monitoring the electronic structure at the Fermi level of the Zn/p-Si(100) system.

Pump-probe XUV photoemission spectroscopy was also employed to investigate the ultrafast charge carrier dynamics at the p-Si(100) substrate decorated with Zn clusters. No ultrafast charge transfer from the p-Si(100) substrate to the smallest Zn clusters (0.03 ML Zn) is observed. This was attributed to the energetic position of the occupied electronic states in Zn, which lead to an ohmic contact at the Zn-p-Si(100) interface that could lead to a negative charging of the clusters upon their formation on the p-Si(100) substrate without any need for photoexcitation. A charge transfer is observed for the Zn clusters formed by evaporation of 0.12 ML and 0.2 ML Zn on p-Si(100), because at these coverages the electronic structure of the cluster leads to the formation of a Schottky barrier at the Zn-p-Si(100) interface and possible to a favorable built in electric field. The relaxation time constants increase with the cluster size, which is in agreement with the previous ultrafast charge carrier dynamics investigations in metal nanoparticles in solutions and embedded in matrices.

## Acknowledgements

The authors gratefully acknowledge financial support provided by the U.S. Air Force Office of Scientific Research (Grant FA9550-14-1-0154). We thank Dr. Bill Flounders from Berkeley Marvell Nanofabrication Laboratory for providing the silicon substrate.

## References


1. Maeda, K.; Teramura, K.; Lu, D.; Takata, T.; Saito, N.; Inoue, Y.; Domen, K. *Nature* **2006,** 440, 295-295.
2. Chen, X.; Shen, S.; Guo, L.; Mao, S. S. *Chem. Rev.* **2010,** 110, 6503-6570.
3. Maeda, K.; Domen, K. *J. Phys. Chem. C* **2007,** 111, 7851-7861.
4. Habisreutinger, S. N.; Schmidt-Mende, L.; Stolarczyk, J. K. *Angew. Chem. Int. Ed.* 52, 7372-7408.
5. Yadav, H. M.; Kim, J.-S.; Pawar, S. H. *Korean J. Chem. Eng.* **2016,** 33, 1989-1998.
6. He, W.; Huang, H.; Yan, J.; Zhu, J. *J. Appl. Phys.* **2013,** 114, 204701.
7. Lilja, M.; Forsgren, J.; Welch, K.; Åstrand, M.; Engqvist, H.; Strømme, M. *Biotechnol. Lett* **2012,** 34, 2299-2305.
8. Mahlambi, M. M.; Ngila, C. J.; Mamba, B. B. *J. Nanomater.* **2015,** 2015, 29.
9. Wang, C.-C.; Li, J.-R.; Lv, X.-L.; Zhang, Y.-Q.; Guo, G. *Energy Environ. Sci.* **2014,** 7, 2831-2867.
10. Peters, S.; Peredkov, S.; Balkaya, B.; Ferretti, N.; Savci, A.; Vollmer, A.; Neeb, M.; Eberhardt, W. *Rev. Sci. Instrum.* **2009,** 80, 125106.
11. Häkkinen, H.; Moseler, M.; Kostko, O.; Morgner, N.; Hoffmann, M. A.; v. Issendorff, B. *Phys. Rev. Lett.* **2004,** 93, 093401.
12. Issendorff, B. v.; Cheshnovsky, O. *Annu. Rev. Phys. Chem.* **2005,** 56, 549-580.
13. Vinod, C. P.; Kulkarni, G. U.; Rao, C. N. R. *Chem. Phys. Lett.* **1998,** 289, 329.
14. Xu, C.; Oh, W. S.; Liu, G.; Kim, D. Y.; Goodman, D. W. *J. Vac. Sci. Technol., A* **1997,** 15, 1261-1268.
15. Bettac, A.; Kœller, L.; Rank, V.; Meiwes-Broer, K. H. *Surf. Sci.* **1998,** 402-404, 475.
16. Hu, M.; Hartland, G., *Ultrafast Dynamics of Metal Nanospheres and Nanorods*. Springer US: 2003.
17. Aeschlimann, M.; Bauer, M.; Pawlik, S.; Weber, W.; Burgermeister, R.; Oberli, D.; Siegmann, H. C. *Phys. Rev. Lett.* **1997,** 79, 5158.
18. Vallee, F. *C. R. Acad. Sci.* **2001,** 2, 1469.
19. Sun, C. K.; Vallee, F.; Acioli, L. H.; Ippen, E. P.; Fujimoto, J. G. *Phys. Rev. B* **1994,** 50, 15337.
20. Ogawa, S.; Nagano, H.; Petek, H. *Phys. Rev. B* **1997,** 55, 10869.
21. Knoesel, E.; Hotzel, A.; Wolf, M. *Phys. Rev. B* **1998,** 57, 12812.

22. Del Fatti, N.; Voisin, C.; Achermann, M.; Tzortzakis, S.; Christofilos, D.; Vallee, F. *Phys. Rev. B* **2000,** 61, 16956.
23. Brorson, S. D.; Kazeroonian, A.; Moodera, J. S.; Face, D. W.; Cheng, T. K.; Ippen, E. P.; Dresselhaus, M. S.; Dresselhaus, G. *Phys. Rev. Lett.* **1990,** 64, 2172.
24. Bloemer, M. J.; Haus, J. W.; Ashley, P. R. *J. Opt. Soc. Am. B* **1990,** 7, 790.
25. Flytzanis, C.; Hache, F.; Klein, M. C.; Ricard, D.; Roussignol, P.; Wolf, E., V Nonlinear Optics in Composite Materials: 1. Semiconductor and Metal Crystallites in Dielectrics: 1. Semiconductor and Metal Crystallites in Dielectrics. In *Progress in Optics*, Elsevier: 1991; Vol. 29, p 321.
26. Miaja-Avila, L.; Lei, C.; Aeschlimann, M.; Gland, J. L.; Murnane, M. M.; Kapteyn, H. C.; Saathoff, G. *Phys. Rev. Lett.* **2006,** 97, 113604.
27. Saathoff, G.; Miaja-Avila, L.; Aeschlimann, M.; Murnane, M. M.; Kapteyn, H. C. *Phys. Rev. A* **2008,** 77, 022903-1 - 022903-16.
28. Frietsch, B.; Carley, R.; Döbrich, K.; Gahl, C.; Teichmann, M.; Schwarzkopf, O.; Wernet, P.; Weinelt, M. *Rev. Sci. Instrum.* **2013,** 84, 075106.
29. Vaida, M. E.; Leone, S. R. *J. Phys. Chem. C* **2016,** 120, 2769-2776.
30. Marsh, B. M.; Vaida, M. E.; Cushing, S. K.; Lamoureux, B. R.; Leone, S. R. *J. Phys. Chem. C* **2017,** 121, 21904-21912.
31. Helander, M. G.; Greiner, M. T.; Wang, Z. B.; Lu, Z. H. *Rev. Sci. Instrum.* **2011,** 82, 096107.
32. Thompson, A. C., *X-ray data booklet*. Lawrence Berkeley National Laboratroy, University of California, Berkeley, 2001.
33. Tanaka, K.-I.; Xie, Z.-X.; Egawa, T.; Aramata, M. *J. Mol. Catal. A: Chem.* **2003,** 199, 19-26.
34. Xie, Z.-X.; Tanaka, K.-i. *Ultramicroscopy* **2005,** 105, 6-11.
35. Yulikov, M.; Sterrer, M.; Risse, T.; Freund, H. J. *Surf. Sci.* **2009,** 603, 1622-1628.
36. Vaida, M. E. A novel technique to monitor ultrafast photoinduced chemical reaction dynamics at surfaces: The femtochemistry of methyl halide molecules adsorbed on oxides, metals and oxide supported metal clusters. university of Ulm, Ulm, 2010.
37. Sze, S. M.; Ng, K. K., *Physics of Semiconductor Devices, 3rd Edition*. John Wiley and Sons Hoboken, 2007.
38. Colinge, J.-P.; Colinge, C. A., *Physics of Semiconductor Devices* Springer: New York, 2006.
39. Kostko, O.; Wrigge, G.; Cheshnovsky, O.; Issendorff, B. v. *J. Chem. Phys.* **2005,** 123, 221102.
40. Siffalovic, P.; Drescher, M.; Heinzmann, U. *Europhys. Lett.* **2002,** 60, 924.
41. Sezen, H.; Ozbay, E.; Aktas, O.; Suzer, S. *Appl. Phys. Lett.* **2011,** 98, 111901-3.
42. Oloff, L. P.; Hanff, K.; Stange, A.; Rohde, G.; Diekmann, F.; Bauer, M.; Rossnagel, K. *J. Appl. Phys.* **2016,** 119, 225106.

43. Kittel, C., *Introduction to Solid State Physics*. Wiley: New York, 1976.
44. Kasap, S.; Capper, P., *Springer Handbook of Electronic and Photonic Materials*. Springer New York, 2006.
45. Rumble, J. R., *CRC Handbook of Chemistry and Physics*. 98th ed.; CRC Press LLC: 2017.
46. Michaelson, H. B. *J. Appl. Phys.* **1977,** 48, 4729-4733.
47. Tatewaki, H.; Tomonari, M. *Can. J. Chem.* **1992,** 70, 642-656.
48. Pacchioni, G. *PCCP* **2013,** 15, 1737-1757.
49. Yoon, B.; Hakkinen, H.; Landman, U.; Worz, A. S.; Antonietti, J.-M.; Abbet, S.; Judai, K.; Heiz, U. *Science* **2005,** 307, 403-407.
50. Kasap, S. O., *Principles of Electronic Materials and Devices*. Third edition ed.; McGraw-Hill Education: 2006.
51. Voisin, C.; Del Fatti, N.; Christofilos, D.; Vallée, F. *J. Phys. Chem. B* **2001,** 105, 2264-2280.
52. Hartland, G. V. *Chem. Rev.* **2011,** 111, 3858-3887.
53. Hu, M.; Hartland, G. V. *J. Phys. Chem. B* **2002,** 106, 7029-7033.

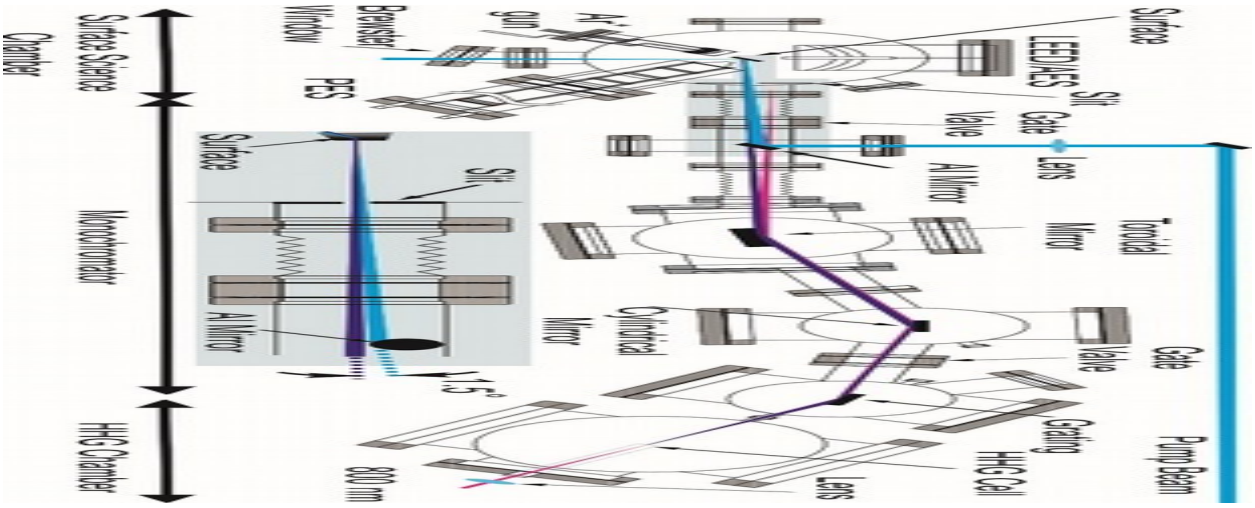


Figure 1. Schematic layout of the experimental setup composed of a fs-XUV source, an XUV monochromator, and a UHV surface science chamber for surface preparation and investigation. Inset: Detail illustrating the overlap between the pump and the probe beams on the surface. See text for more details.

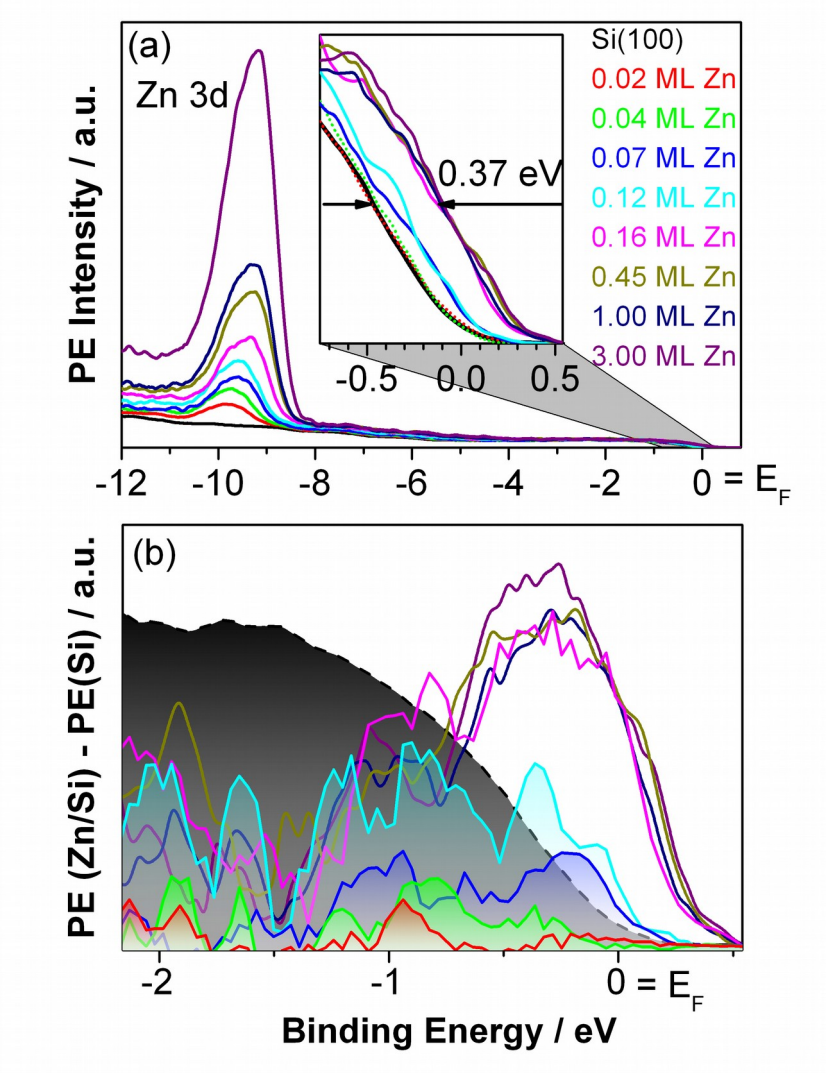


Figure 2 (a) Photoemission spectra recorded with the 27$^{th}$ harmonic from a bare Si(100) surface as well as from a Si(100) surface covered with well-defined amounts of Zn. No background correction is performed for these photoemission spectra. The inset shows a magnified view of the photoemission onset from the spectra displayed in the main figure. (b) Difference between the photoemission spectra obtained from Zn clusters on Si(100) and the photoemission spectrum obtained from the bare Si(100) substrate. The different photoemission spectra from coverages up to 0.12 ML Zn are shaded, to improve the perceptibility of the photoemission features.

The spectrum obtained from the bare Si(100) surface is displayed as a reference (dashed filled curve).

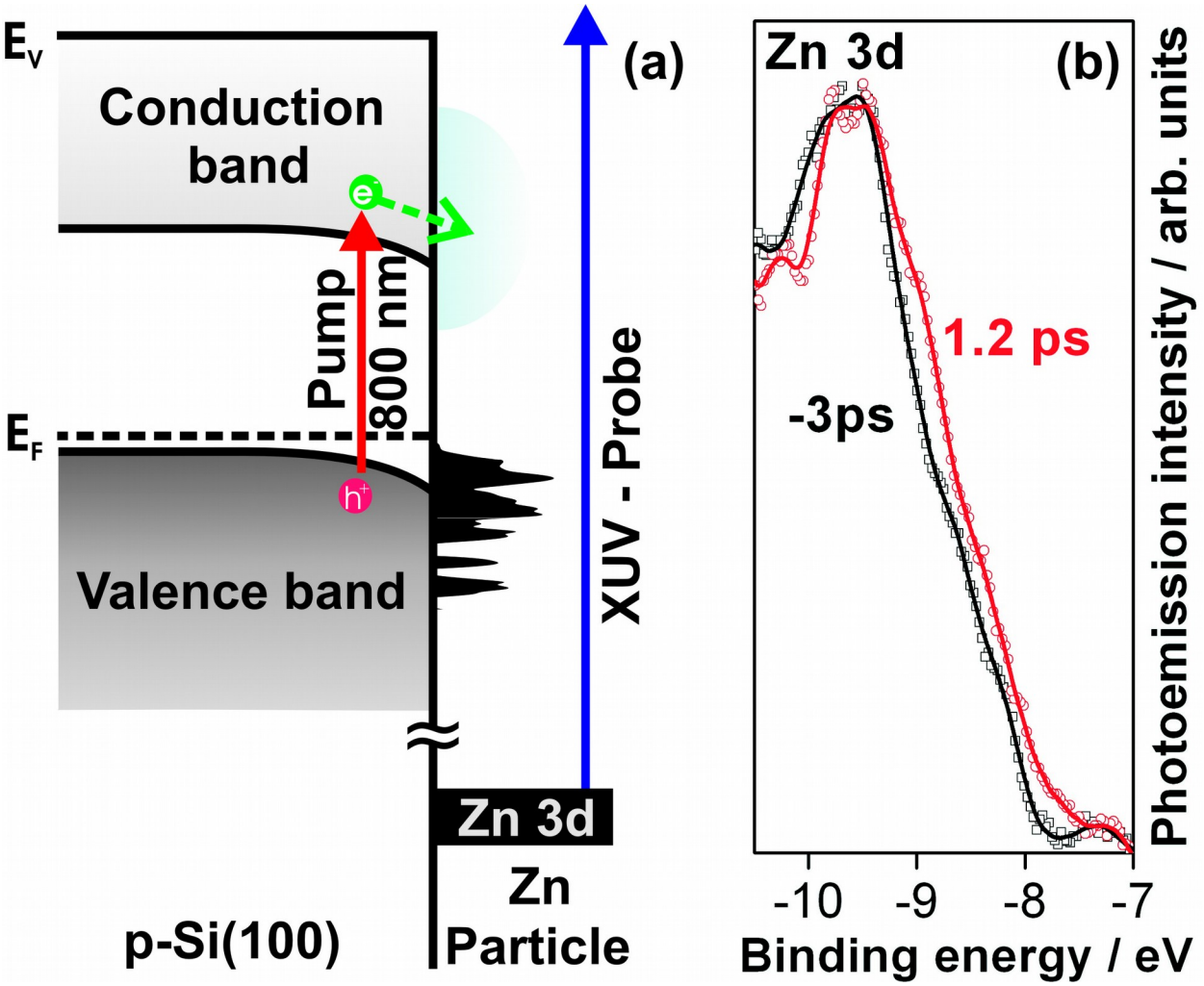


Figure 3. (a) Schematic energy level diagram illustrating the band alignment of a Zn particle on p-Si(100) together with the pump-probe schema used to monitor the charge carrier dynamics at the Zn particles. The red and blue vertical arrows represent the IR-pump and XUV-probe laser pulses, respectively. The dashed curved arrow represent the trajectory of the electron after the photoexcitation of the p-Si(100) substrate and the light blue region represent the unoccupied states of the Zn particle. (b)

Photoemission spectra from 0.12 ML Zn/p-Si(100) recorded with the 23rd harmonic before (-3 ps) and after (1.2 ps) the IR-pump pulse excitation.

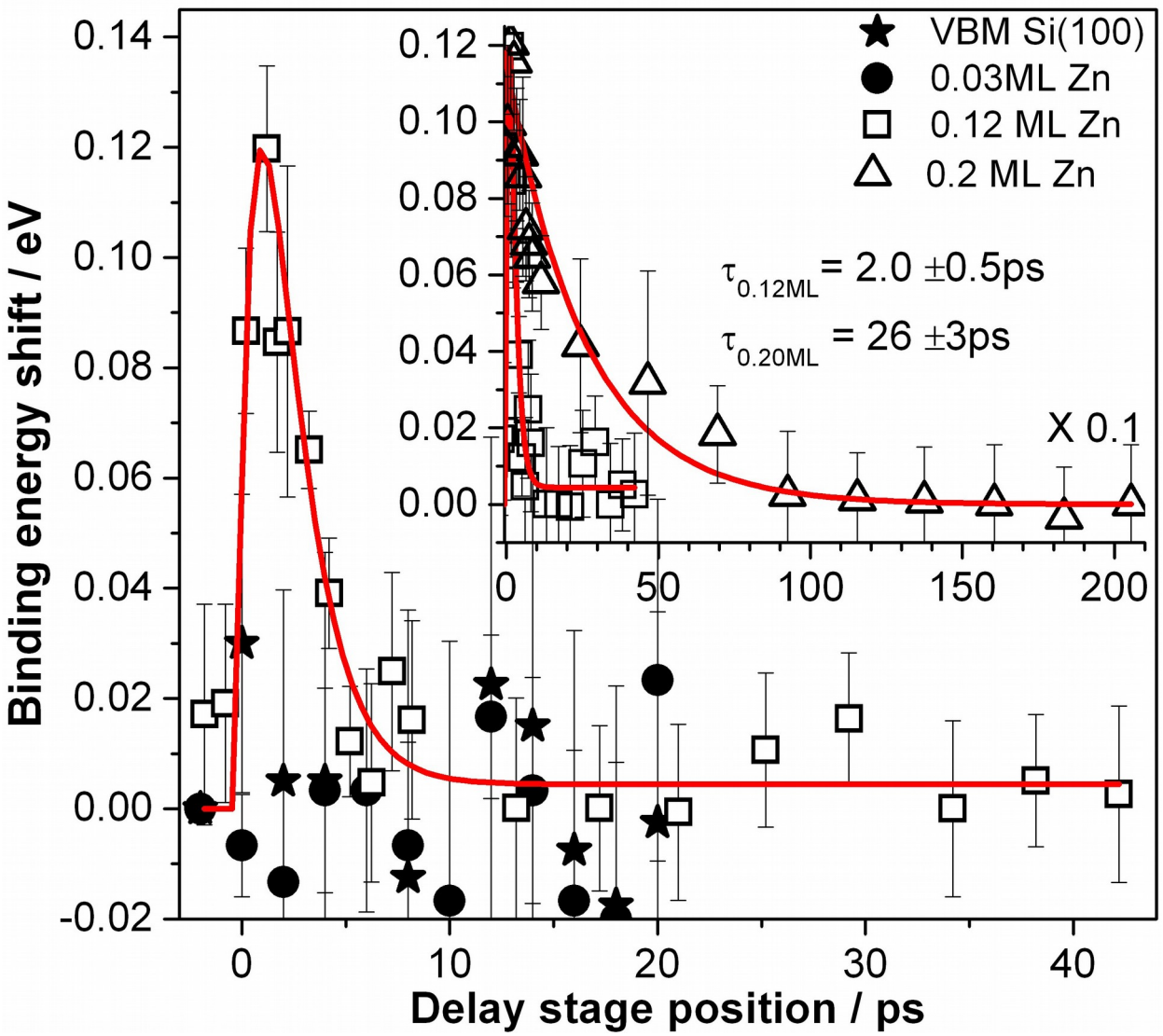


Figure 4. Ultrafast charge carrier dynamics at the surface of a p-Si(100) surface decorated with Zn clusters. Transients obtained from 0.03 ML Zn on Si(100) (filled circles), 0.12 ML Zn/Si(100) (open squares) and 0.2 ML Zn/Si(100) (open triangles) by monitoring the shift of the Zn 3d photoemission peak as a function of the pump (800 nm) - probe (23rd

harmonic) time delay. *The transient signal from 0.2 ML Zn/Si(100) is divided by a factor of 10 (multiplied by 0.1) to match the intensity of the transient signal obtained from 0.12 ML Zn*

A transient signal obtained from the bare Si(100) by monitoring the valence band maximum of p-Si(100) under identical investigation conditions is included as a reference (filled stars).

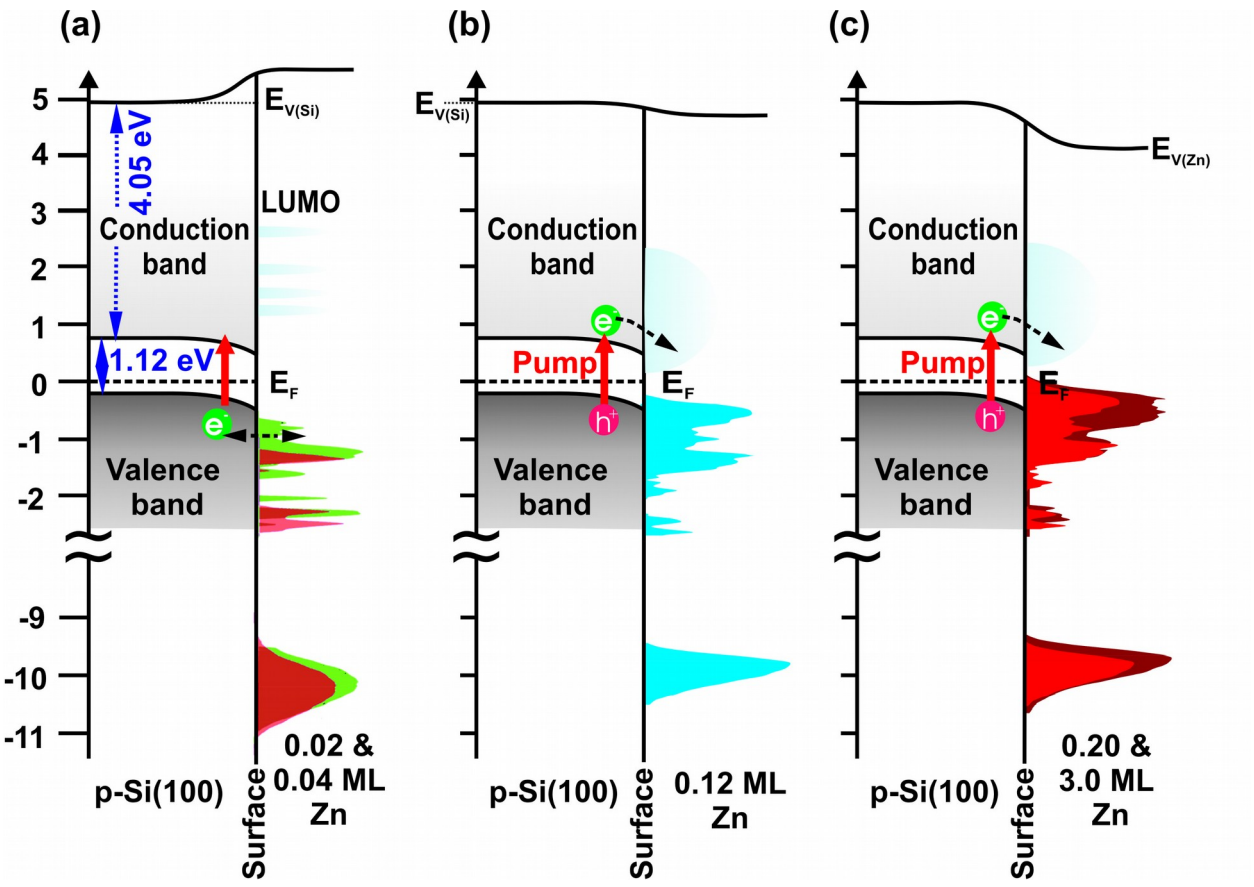

Figure 5. Schematic energy level diagrams illustrating the band alignments between various Zn particles sizes and the Si(100) substrate as well as the mechanisms of electron transfer at the p-Si(100)-Zn interface: (a) 0.02 ML Zn (red) and 0.04 ML Zn (green), (b) 0.12 ML Zn, and (c) 0.2 ML Zn (red) and 3.0 ML Zn (brown). The energetic location of the Fermi energy, valence band maximum of Si(100), occupied electronic states in Zn particles, and Zn 3d states are obtained from the present experiment. The values for the band gap of Si, conduction band width (electron affinity) of Si(100) and Zn are taken from Refs.. The occupied electronic states of Zn on the right side of each panel are normalized spectra taken from the inset in Figure 2. The light blue regions on the right side of each panel are repesenting the unoccupied electronic states in the Zn particles.

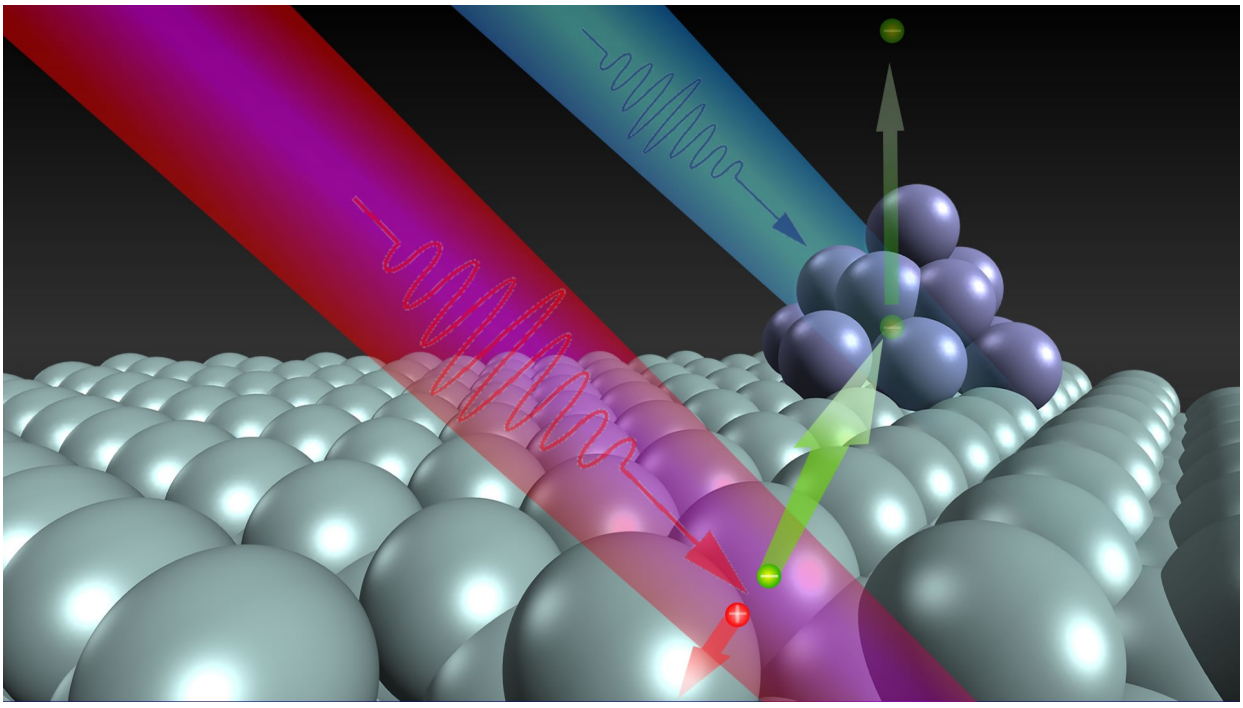

Graphical abstract